Optics Communications 547 (2023) 129850

Contents lists available at ScienceDirect

Optics Communications

journal homepage: www.elsevier.com/locate/optcom

Improved underwater wireless optical communication using a passively mode-locked VECSEL

Tao Wang [a], Ruiyang Tian [a], Renjiang Zhu [a], Lidan Jiang [a], Cunzhu Tong [b], Huanyu Lu [b], Yanrong Song [c], Peng Zhang [d,*]

[a] College of Physics and Electronic Engineering, Chongqing Normal University, Chongqing, 401331, China
[b] Changchun Institute of Optics, Fine Mechanics and Physics, Chinese Academy of Sciences, Changchun, Jilin, 130033, China
[c] Faculty of Sciences, Beijing University of Technology, Beijing, 100124, China
[d] National Center for Applied Mathematics, Chongqing Normal University, Chongqing, 401331, China

ARTICLE INFO

Keywords:
Underwater wireless optical communications
Vertical-external-cavity surface-emitting laser
Mode-locked
QC-LDPC
PPM

ABSTRACT

This paper presents improved underwater wireless optical communication (UWOC) based on a 490 nm passively mode-locked vertical-external-cavity surface-emitting laser (VECSEL) with the repetition rate of 1.46 GHz and the pulse width of 2.25 ps. After conducting a comprehensive evaluation of the performance characteristics of quasi-cyclic low-density parity-check (QC-LDPC) coding and pulse-position modulation (PPM) in relation to bit-error-rate (BER) and communication capacity across different signal-to-noise ratios (SNRs), a passively mode-locked VECSEL based UWOC system is designed and experimentally performed. The UWOC system employs the QC-LDPC encoding technique and PPM modulation scheme that are most suitable for the system. Compared with the case without QC-LDPC, the minimum received optical power with coding is improved by 3.5 dBm, and the SNR with coding is improved by 0.4 dB under condition of 256-PPM and forward error correction (FEC) threshold of 3.8×10^{-3}. Meanwhile, compared with the UWOC system using a continuous-wave (CW) VECSEL as the light source, the attenuation coefficient of the UWOC system based on the mode-locked VECSEL is decreased by 0.04 m^{-1}, and the BER of the mode-locked VECSEL based UWOC system is decreased by 0.3 dB.

1. Introduction

Underwater communication networks provide an important role for environmental recording, biological observation, underwater equipment detection and pollution control [1–3]. However, conventional acoustic and radio frequency (RF) communication cannot simultaneously satisfy long-range underwater communication at MHz transmission rate because of their low transmission rate or high underwater attenuation [4,5]. In recent years, underwater wireless optical communication (UWOC) has been widely used to high-speed, long-distance, and power-limited underwater communication because of its characteristics of low-power consumption and high bandwidth [6].

Various forms of coding and modulation can be introduced in an UWOC system. The most frequently used coding in an UWOC system is error-correcting codes, whose aim is to improve the transmission quality of the underwater channel. The common error-correcting codes include linear block codes, cyclic codes, Reed-Solomon (RS) codes, convolutional codes, etc. [7–9]. The QC-LDPC used in this work is one of the linear block codes.

For modulation, the reported researches show that the UWOC systems using higher-order modulation formats have difficulty in achieving long-distance communication despite of obtaining Gbps transmission rates [10–12]. Therefore, direct modulation technique is considered by more researchers as the communication modulation format for long-range UWOC. Direct modulation converts the information into light intensity by modulate the driving current of the laser. The main modulation methods include On-Off Keying (OOK), PPM, pulse amplitude modulation (PAM), etc. Because the direct modulation based on the PPM has higher power efficiency and better noise immunity at the same BER. Therefore, it is more suitable for medium to long distance underwater communication than other direct modulation formats [13–16].

Table 1 shows the relevant researches of the UWOC system based on PPM. In long distance communication [17,18,21], the PPM was difficult to achieve high rate [22] or narrow pulse [6] because of pulse stretching, which is mainly caused by the scattered particles and plankton [17]. But for engineering application, the transmission rate of Mbps has already

* Corresponding author.
E-mail address: zhangpeng2010@cqnu.edu.cn (P. Zhang).

https://doi.org/10.1016/j.optcom.2023.129850
Received 12 June 2023; Received in revised form 7 August 2023; Accepted 20 August 2023
Available online 23 August 2023

Table 1
Researches of PPM UWOC system.

Years	Light source	Data rate/Pulse width	Distance	Detector	Modulation	Power
2018 [17]	LD	1.7 Mbps	120 m	SPAD	256-PPM	1 mJ/1.5 KHz
2018 [18]	LD	5 Mbps	46 m	MPPC	4-PPM	0.17 mW
2021 [19]	LED	5 Mbps	1.5 m	SPAD	256-PPM	–
2021 [20]	LD	6.21 Mbps	2 m	SPAD	4-PPM	75 mW Peak power
2022 [21]	MOPA	9.14 Mbps	99 m	PMT	64-PPM	600 mW
2022 [22]	LED	50 Mbps	2 m	APD	8-PPM	–
2022 [6]	LD	200 ps	7 m	PD	64-PPM	−4.4 dB
2023 [34]	LD	12.5 Mbps	5 m	PCM	32-PPM	0.47 mW
This work	VECSEL	20 ns	18 m	APD	256-PPM	15.6 mW

met the requirement of underwater communications. Now, how to improve the communication quality and transmission distance should be the more reasonable target for an UWOC system with PPM. One method to enhance the quality of a signal is through the utilization of phase compensation. [33]. In addition, it also can be seen from Table 1 that the single-photon detection technique is suitable for longer distance communication [6,17–20,34], but finding a single-photon in ocean is a great challenge. On comparison, using conventional detection and efficient light source to achieve long-distance underwater communication is a mean of communication more in line with the actual underwater environment.

From Beer-Lambert law, it is known that the attenuation of optical power exponentially increases with the enlarged transmission distance. However, it is not so cost-effective to increase the communication distance by increasing the power [23]. In 2009, Linda et al. reported an underwater scattering experiment using a 532 nm mode-locked laser, and found that the forward scattering was reduced with an increased repetition rate of the laser pulse [24]. Brandon et al. got similar results in 2017 [35]. This means that a mode-locked laser with high repetition frequency will be more suitable for long distance underwater transmission. However, as the Table 1 shows that the light sources used in most of the studies were commercial CW lasers, there were few researches on UWOC using pulse light source. In 2018, Hu et al. achieved 120 m transmission distance by a solid-state laser with a repetition frequency of 1.5-kHz, corresponding a link loss of 136.8 dB [17]. Due to their relatively low repetition frequency (∼1.5 kHz), and the pulse width of PPM must match to the corresponding repetition frequency, so this will limit the actual utilization of the UWOC system. Obviously, there is necessary to employ a pulsed laser with short pulse duration and high repetition frequency for UWOC system.

As a new type of semiconductor laser, VECSEL has advantages such as high output power and good beam quality. The flexible external cavity also allows placing a semiconductor saturable absorber mirror (SESAM) for mode-locking, so to produce a short pulse duration and high repetition rate [25–30]. Therefore, it can provide a reliable light source for studying the transmission and communication performance of pulsed light in UWOC.

In this work, we designed a 490 nm mode-locked VECSEL based UWOC system with QC-LDPC codes and PPM. In order to get an optimized coding strategy, the influence of QC-LDPC parameters on BERs is simulated and analyzed. Then the performance of BERs is tested with ∼18 m underwater channels and different Maalox suspension solutions. The results show that 1/2 code rate and 256-PPM are the most suitable coding strategies in higher scattering environments. While in low scattering environments, 1/2, 2/3, 3/4 code rates and 64-PPM can be used for UWOC systems considering bandwidth utilization and coding resources consumption. The experimental results are in good agreement with the simulation. Finally, a CW VECSEL based UWOC system is built to compare with the mode-locked VECSEL based UWOC system, and the attenuation coefficient obtained by the latter is about 0.04 m^{-1} less than that of the former, showing an improved underwater channel performance.

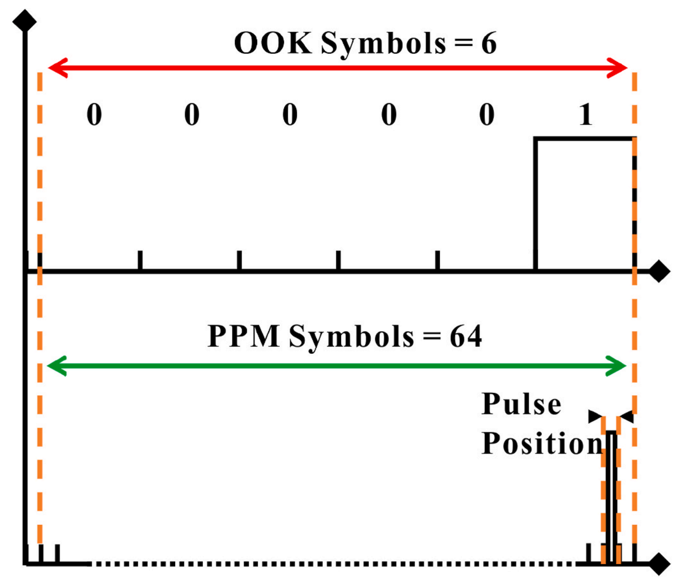

Fig. 1. 64-PPM and OOK mapping relationship.

2. Theory and simulation

2.1. PPM and QC-LDPC codes

In PPM, the relatively high energy efficiency and pulse power are obtained at the expense of spectral efficiency, so that in systems with insufficient bandwidth (e.g., high-speed wireline communications), it is less competitive. However, due to the relatively abundant channel bandwidth in UWOC, PPM becomes an attractive modulation method especially in long-distance communication where the reliability of data communication becomes the most important aspect. Fig. 1 expresses the principle and structural composition of PPM and OOK mapping as an example of 64-PPM. The transmitted information is represented by the position of the pulse in the symbol, corresponding to the decimal value of the M input symbols.

The LDPC code defined in the IEEE802.16e standard is a quasi-cyclic non-regular LDPC code with four rates. Each rate has a corresponding checksum matrix H. H_b is the base check matrix of H. H_b is expanded to obtain H. The size of H_b is $m_b \times n_b$, and the composition is shown in equation (1).

$$H_b = [H_{b1} \quad H_{b2}] \tag{1}$$

The length of n_b is fixed to 24 and the length of m_b varies according to the code rate. Hb1 is an $m_b \times (n_b - m_b)$ matrix. H_{b2} is an $m_b \times n_b$ matrix. And q is called the expansion factor, H_b can be obtained by expanding the check matrix H by $m_b \cdot q \times n_b \cdot q$. The elements in H_{b1} consist of -1 or non-negative integers. If it is -1, the corresponding position of the check matrix H is an all-0 matrix; if it is a non-negative integer, the corresponding position of the check matrix H is the matrix obtained by

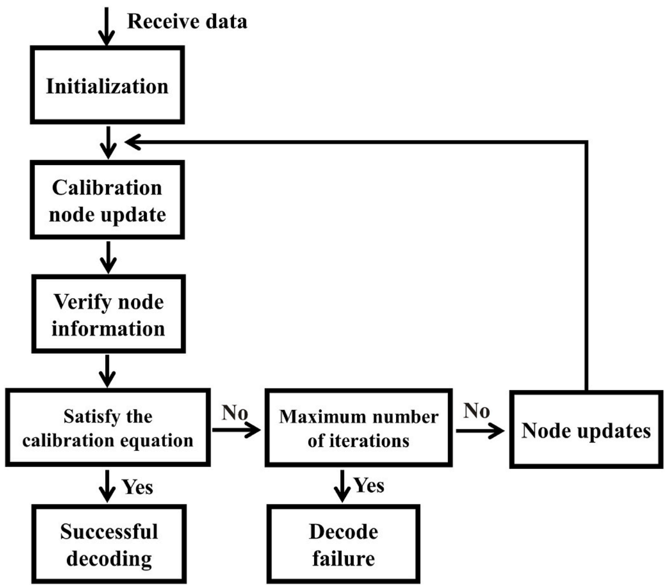

Fig. 2. Schematic of QC-LDPC decoding.

shifting the unit matrix E by non-negative integer times to the right. H_{b2} forms a quasi-bidiagonal structure except for the first column, where the elements on the two quasi-diagonal lines are 0 and the other positions are -1. The elemental composition of H_{b2} is shown in equation (2).

$$H_{b2}=\begin{bmatrix} h(1) & 0 & & & & & & \\ -1 & 0 & 0 & & & & & \\ \vdots & & 0 & 0 & & -1 & & \\ -1 & & & 0 & \ddots & & & \\ h(r) & & & & \ddots & \ddots & & \\ -1 & & & & & \ddots & 0 & \\ \vdots & & & & & & 0 & 0 \\ -1 & & & & & & & 0 \quad 0 \\ h(m_b) & & & & & & & \quad\ 0 \end{bmatrix}_{m_b\times n_b} \tag{2}$$

Let the element in the base check matrix at position (i, j) be $q(i, j)$, and the update method of $q(i, j)$ is shown in equation (3). And the k is taken differently in different code lengths.

$$q(i,j)=\begin{cases} q(i,j), q(i,j)\le 0 \\ \left\lfloor \dfrac{q(i,j)\cdot q}{p} \right\rfloor, q(i,j)>0 \end{cases} \tag{3}$$

The algorithm of channel decoding is an important factor in determining the coding performance and application scope, and an important reason for the attractiveness of LDPC codes is the advantage of the decoding algorithm. LDPC code is a packet code based on a sparse check matrix, which makes it possible to overcome the huge computational effort faced by packet codes in long codes. At the same time, the sparse matrix property makes the consecutive burst errors have little effect on the decoding code. LDPC coding is very close to the Shannon's limit [36], and its good error correction ability in burst error channels makes it very suitable for high-speed optical communication. And the algorithm can be implemented in parallel operation and has the advantages of low hardware implementation difficulty. The main algorithm for LDPC codes is the Back Propagation (BP) algorithm. It is often used for soft decision, but it can also be implemented with hard decision. the form of message delivery in BP algorithm is log-likelihood ratio (LLR), and the iterative decoding process is the delivery and updating of data between check message nodes. As a structured LDPC code, QC-LDPC code follows a certain regularity in its check matrix, which is simple in structure, easy to implement, and has lower coding complexity compared with random LDPC code. Fig. 2 is a block diagram of QC-LDPC decoding process based on BP-Log-decoding. After receiving signal Y =

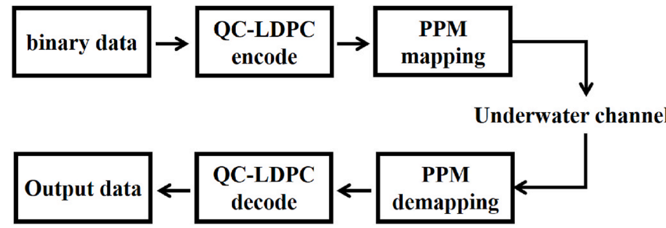

Fig. 3. Schematic of the QC-LDPC and PPM UWOC system through an underwater channel.

$\{y_1, y_2, \ldots, y_n\}$ from the underwater channel, the initialization process is executed first as equation (4):

$$Z_{mn}=LLR_n^{(0)}=2y_n/\delta^2, n=0,\ldots,N-1, m\in M(n) \tag{4}$$

Then the check node is updated as in equation (5):

$$L_{mn}^{(k)}=2\tanh^{-1}\prod_{n'\in N(m)\setminus n}\tanh\left(\frac{V_{mn'}^{(k-1)}}{2}\right), n=0,\ldots,N-1, m\in M(n) \tag{5}$$

The bit node is updated as in equation (6):

$$\begin{aligned} & n=0,\ldots,N-1, n\in M(n) \\ & Z_{mn}^{(k)}=LLR_n^{(0)}+\sum_{m'\in M(n)\setminus m} L_{m'n}^{(k)}; \\ & LLR_n^{(k)}=LLR_n^{(0)}+\sum_{m'\in M(n)} L_{m'n}^{(k)} \end{aligned} \tag{6}$$

Subsequent hard decisions of L_{mn} generate decoded data. Here, let m, n denote the rank index of H. Z_{mn} denotes the transmission of information from n^{th} check nodes to m^{th} bit nodes, LLR_n denotes the log-likelihood ratio of the codeword, and k denotes the number of iterations.

2.2. Simulation of coding capability

Fig. 3 shows a schematic of the UWOC system with QC-LDPC and PPM through an underwater channel. At the transmitter side, the pseudo-random-binary data stream is framed according to the IEEE.802.16 standard, and the code length of each frame is m (the value of m is taken as 576, 1152, 2304) for QC-LDPC encoding, and the number of check bits of the encoding is taken as 1/2, 1/3, 1/4, and 1/6 of the code length, respectively. Then the PPM mapping of the framed data stream is performed to obtain the modulated signal before entering the underwater channel. The noise in the underwater channel is simulated using additive white Gaussian noise. At the receiver side, the received optical signal is demodulated by PPM and decoded by QC-LDPC to obtain the signal after transmission through the channel.

Fig. 4(a) simulates the BERs of QC-LDPC at different iterative times. The trend of the curve shows that the BERs quickly decrease as the iterations increases from one to ten times. Subsequently, the efficiency of the BERs transformation slowly decreases when the iterations are greater than ten times. Therefore, considering the computational resources, we finally choose ten iterations as the experimental parameter. Fig. 4(b) shows the simulation results of the BERs of QC-LDPC with different code lengths. It can be seen that the BERs decrease with the code length increasing from 576 to 2304, so in terms of code length, we finally choose a code length of 2304 as the experimental condition.

The BERs of QC-LDPC with different code rates at 256-PPM was simulated, as shown in Fig. 5. The 10^8 symbol simulation tests are performed for all coding strategies. For QC-LDPC coding, we test the simulations of LDPC (2304,1152), LDPC (2304,1536), LDPC (2304,1728), and LDPC (2304,1920). The number of error correction matrices corresponding to these four code types are 1152, 768, 576, and 384. From the theory, it is clear that the error correction capability is more robust when there are more error-correcting codes. Simulation

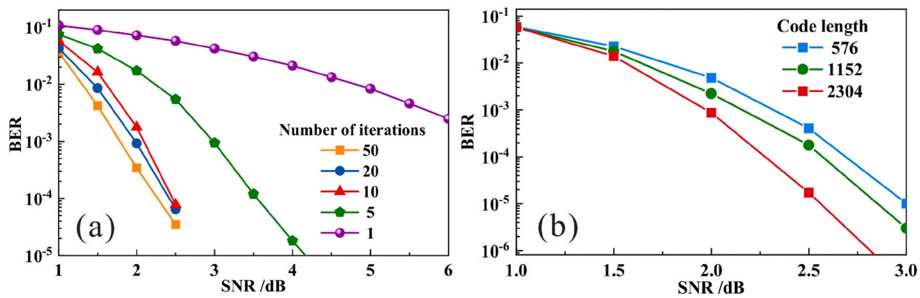

Fig. 4. (a) BERs of QC-LDPC at different iterations. (b) BERs of QC-LDPC with different code lengths.

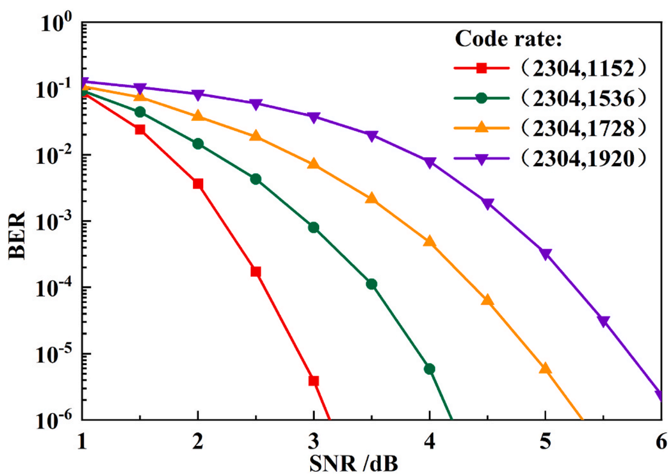

Fig. 5. BERs performance of QC-LDPC with different code rates.

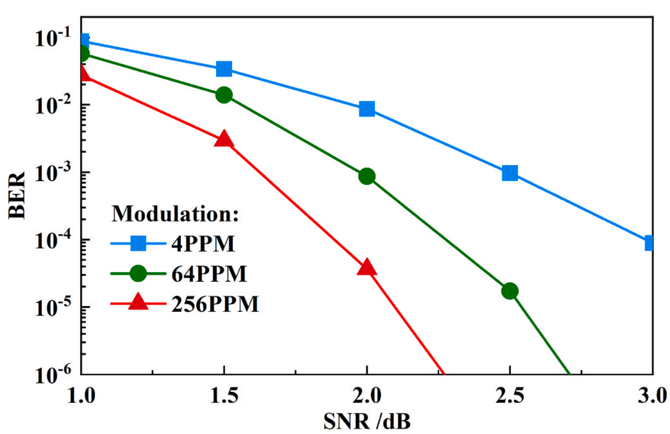

Fig. 6. BERs performance of PPM at different orders.

results also verify this, with the same code length (i.e., 2304 symbols), 1152 error-correcting codes have the lowest BER at the same signal-to-noise ratio. As the amount of valid data increases, the number of error correction codes decreases, leading to a gradual rise in BER, with the highest BER observed in LDPC (2304,1920).

With the results of the previous simulations, we found that the suitable computational volume and excellent BER performance can be obtained when the number of iterations is 10 times, the code length is set to 2304, and the code rate is 1/2. Subsequently, the PPM of different orders are shown in Fig. 6. 256-PPM has lower BER performance than other lower PPM order at code lengths of (2304,1152). Since the pulse width of all modulated signals in this experiment is constant, when the modulation order of PPM is increased, the corresponding transmission time per bit of the baseband signal increases, thus the baseband signal rate decreases. As a directly result, the inter-symbol interference (ISI) also decreases, which lead to the lower BER in Fig. 6.

3. Experiments and discussions

3.1. 490 nm mode-locked VECSEL

The experimental setup of the 490 nm mode-locked VECSEL is shown in Fig. 7(a). The heatsink is mounted to a thermal-electronic cooler, which is connected with a water-cooling system to keep the temperature at 15 °C. A V-shaped resonant cavity is formed by the distributed Bragg reflection (DBR) at bottom of the gain chip and another DBR at bottom of the SESAM, and a folded mirror with 50 mm curvature radius and high-reflectivity (99.9%) at 980 nm is used as the output coupler. The pump source is an 808 nm fiber-coupled semiconductor diode laser with 11.5 W output power, and the core diameter of its pigtail fiber is 100 μm. We use a 1:1 imaging lens pair to focus the pump beam on gain chip at an incident angle of about 30°, and this will deliver a pump spot with diameter of about 100 μm on gain chip, approximately matching to the laser spot.

Then a 5 mm length lithium borate (LBO) crystal is inserted in the arm that include the SESAM for frequency-doubling. The crystal should be situated close to the SESAM as can as possible, so to produce a smaller laser spot on crystal and obtain higher conversion efficiency of frequency-doubling. It should be noted that the inserted crystal may destroy previously mode-locking, and some further adjustments of the cavity are needed to maintain the mode-locking. Spectra of the frequency-doubled mode-locked VECSEL are measured using a spectrometer (HORIBA iHR320, 150–1500 nm wavelength range, 0.06 nm resolution) and the data are shown in Fig. 7(b). The fundamental laser wavelength is 980 nm and the frequency-doubled laser wavelength is 490 nm.

To start the mode-locking, the SESAM should be saturated before the gain medium. Thus, the lengths of the arm containing the gain chip and the arm including the SESAM are selected to be 65 and 38 mm, respectively, which makes the ratio of the spot area on the gain chip and the SESAM to be about 25:1. By slightly adjusting the output coupler or fine tuning the arm length between the output coupler and SESAM, the stable continuous mode-locked pulses can be produced. A high-speed free space detector (Thorlabs DET08C, 5 GHz bandwidth, 800–1700 nm waveband) is used to receive the output pulses, then the signal is delivered to a mixed signal oscilloscope (Tektronix MSO68B, 10 GHz bandwidth, 50 GHz sampling frequency) for showing the pulse train. The observed mode-locked pulse train is plotted in Fig. 8, and the inset indicates pulses in 200 ns time range.

The repetition rate of the mode-locked pulses is recorded by an electrical spectrum analyzer (ESA, RIGOL DSA800, 7.5 GHz bandwidth). The measured RF spectrum can be found in Fig. 9(a). The fundamental signal of 1.46 GHz is strictly corresponding to the cavity length of 103 mm. We also measure the beam quality of the mode-locked laser using a M^2 measurement system (Thorlabs M2MS-BC106 N), and the results are

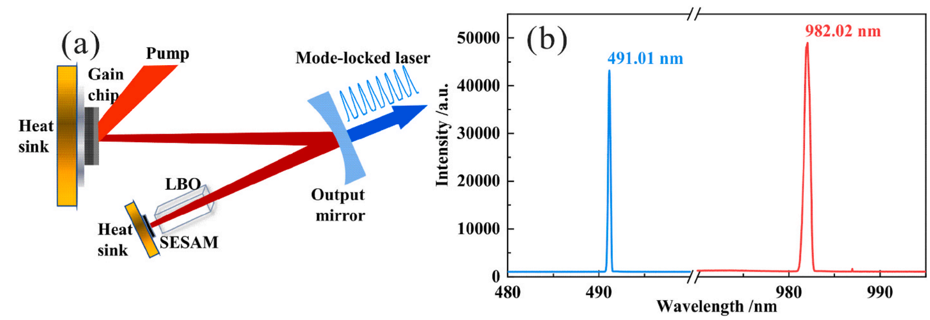

Fig. 7. (a) Schematics of the SESAM mode-locked VECSEL. (b) Spectra of the frequency-doubled mode-locked VECSEL.

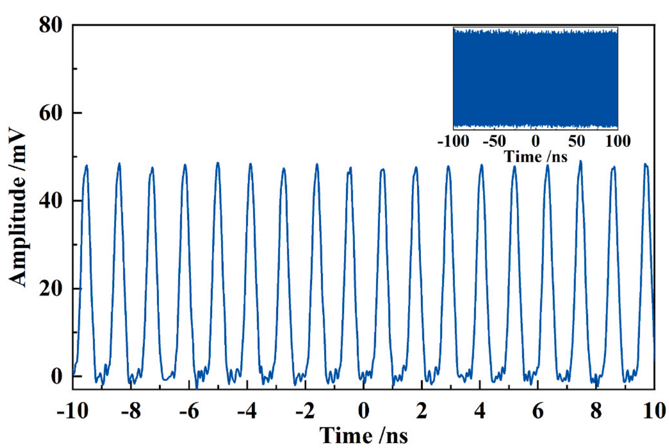

Fig. 8. Pulse train of the mode-locked VECSEL. The inset shows the pulses in 200 ns time range.

shown in Fig. 9(b). The M^2 factors on x and y directions are 1.03 and 1.00 respectively, indicating a good beam quality of the SESAM mode-locked VECSEL.

3.2. VECSEL based UWOC system

The schematics of the experimental UWOC system with a 490 nm mode-locked VECSEL based on acousto-optic modulator (AOM, SGT250-490-0.2 TA) using PPM is shown in Fig. 10. The modulation signal is generated by an arbitrary waveform generator (AWG, Tektronix AWG70002A, 50 Gs/s sampling rate, 2 Gs record length), and loaded into the piezoelectric transducer by the acousto-optic driver, which can modulate the phase and frequency of the light entering into the AOM. A focusing lens with shorter focal length ($f1$=75 mm) is used to focus the 490 nm mode-locked VECSEL before it entering the AOM, and another lens with longer focal length ($f2$=300 mm) is employed on the other side to expand the laser beam to reduce its divergence. We measured the average power of the mode-locked laser output to be 12 dBm and the pulse energy to be 1.03×10^{-11} J. Then, the 490 nm mode-locked VECSEL with modulated signal enters the water tank for transmission, while plane reflectors are used to increase the transmission distance in the water. By increasing or decreasing the number of plane reflectors, the laser output power can be recorded at different distances. And the output laser power was measured using a power meter (Thorlabs PM100D) and detector (Thorlabs S140C, 5 mm aperture, wavelength 350–1100 nm, power range 0.001–500 mW). The output beam is focused onto an avalanche photodetector (APD, Thorlabs APD210, 400–1000 nm wavelength range, 5–1600 MHz bandwidth, 0.5 mm active area diameter) by a lens. Finally, a mixed signal oscilloscope (MSO, Tektronix MSO68B, 10 G bandwidth, 50 Gs/s sampling rate) is used to record and analyze the received signal.

3.3. Results and discussions

In our previous work, we have reported the UWOC system with an acousto-optic crystal for external modulation [31]. The incident angle has a significant effect on the diffraction efficiency (i.e., modulation depth and diffraction separation angle) and the modulation pulse width. Therefore, we explored the modulation depth using different incident angles, as shown in Fig. 11(a). It can be seen that the maximum modulation depth is available at angle of $\pm1.817^\circ$. Fig. 11(b) shows the modulation pulse width of PPM that can be achieved by the AOM under stable communication conditions, corresponding the minimum pulse width is 20 ns.

Fig. 12(a) shows the BERs performance of 256-PPM based UWOC system in different Maalox suspension concentrations with different code rates (i.e., QC-LDPC (2304,1152), QC-LDPC (2304, 1536), QC-LDPC (2304, 1728), QC-LDPC (2304,1920)). The Maalox suspension composed mainly of Al $(OH)_3$ and Mg $(OH)_2$, corresponding a solution ratio of 220 mg/5 mL and 195 mg/5 mL [32]. On the whole, it can be found that BERs decrease with the increase of the number of error correction codes. This rule is consistent with the simulation results.

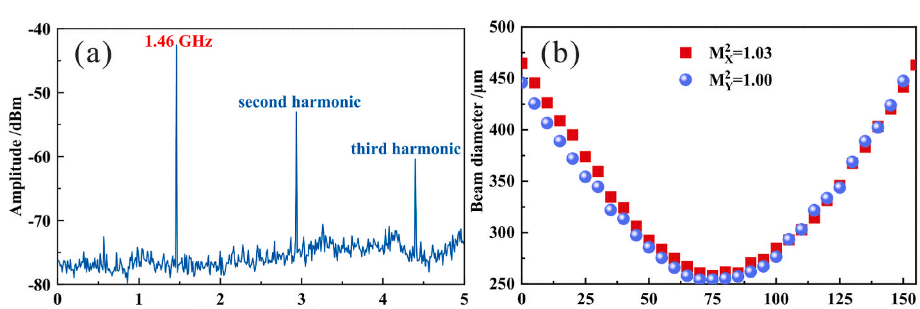

Fig. 9. (a) RF spectrum of the mode-locked VECSEL. The second and the third harmonic are also plotted. (b) Measured M^2 factor of the output beam of the mode-locked VECSEL.

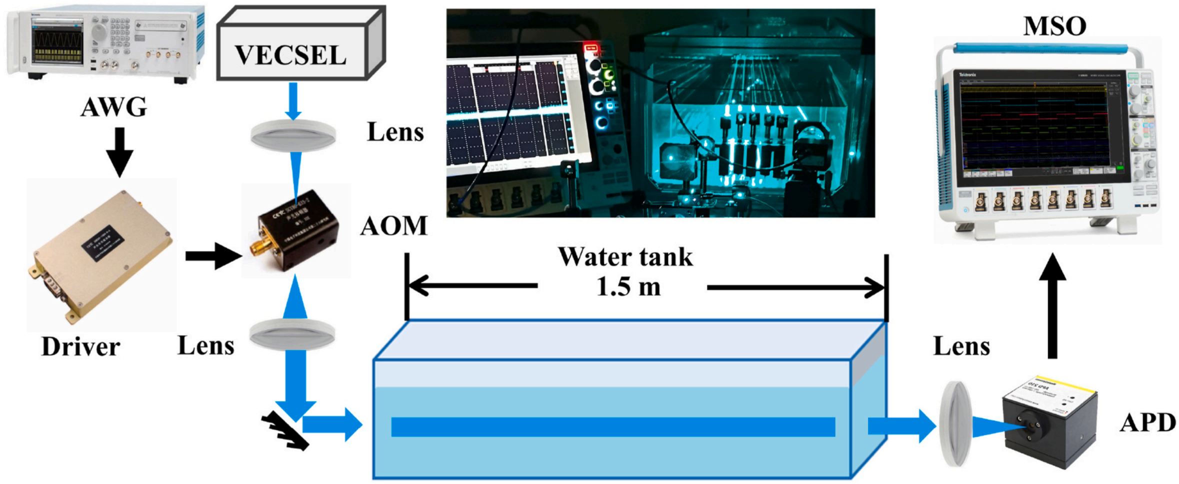

Fig. 10. Experimental setup of the VECSEL based UWOC system.

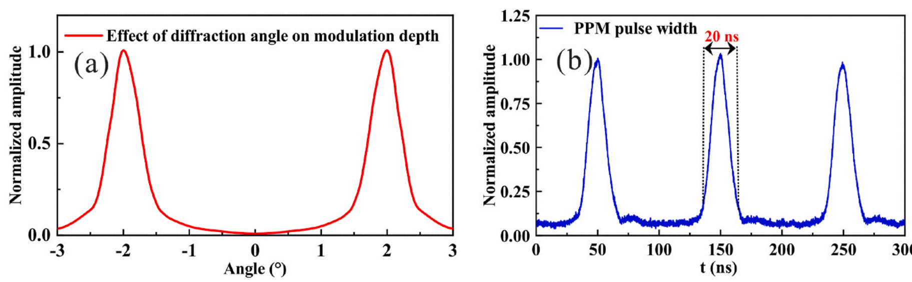

Fig. 11. (a) Modulation depth of incident light at different incident angles. (b) Pulse width based on PPM.

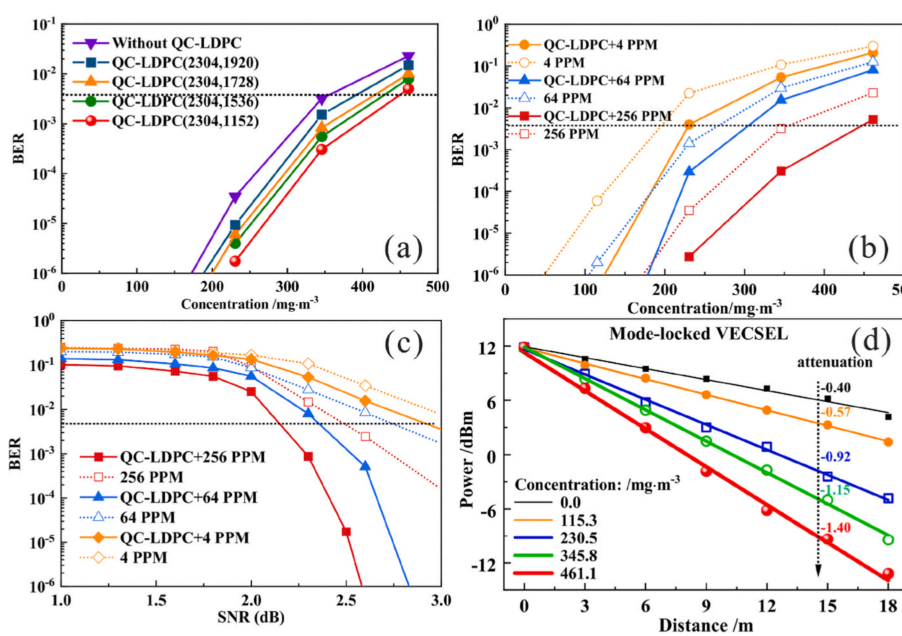

Fig. 12. (a) The evolution of BERs with solution concentration at different code rates. (b) BERs performance of PPM with and without QC-LDPC codes at different Maalox concentrations. (c) BERs performance of PPM with and without QC-LDPC codes at different SNRs. (d) Power attenuation of mode-locked laser with different distance.

Because the experimental environment is not AWGN channel, there is a gap between experiment and simulation. For the 18 m distance communication, the BERs of the 0 mg m^{-3} and 115.3 mg m^{-3} are all less than 1×10^{-6}, all encoding strategies exhibit excellent performance. Subsequently, the BERs began to increase gradually with the Maalox suspension concentrations increased, and the threshold conditions of FEC can be met before 345.8 mg m^{-3}.

Fig. 12(b) shows the BERs performance of UWOC system based on

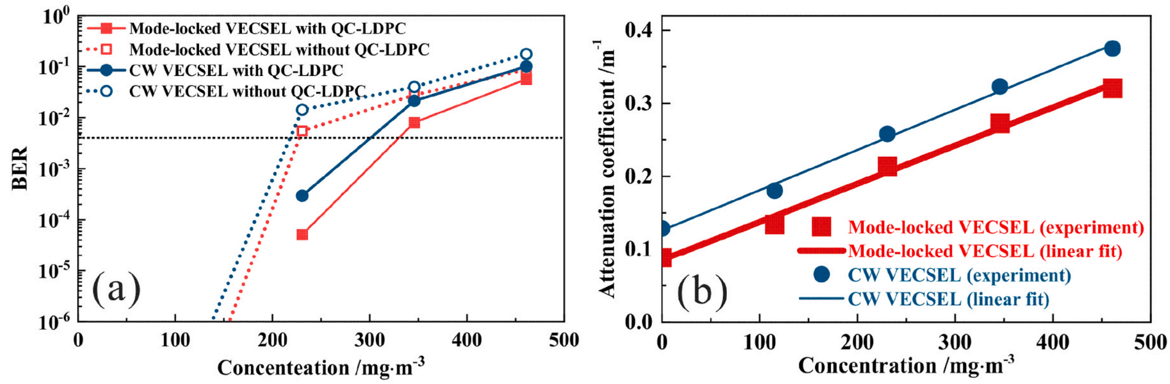

Fig. 13. (a) BERs of CW and mode-locked laser under QC-LDPC (2304,1152) coding and 64-PPM at different concentrations. (b)Attenuation coefficients of CW and mode-locked lasers at different concentrations.

with and without the QC-LDPC and PPM in different Maalox suspension concentrations. It can be seen that the BERs will decrease with the increasing of PPM order. Moreover, adopting QC-LDPC coding could also effectively reduce BERs. For example, compared with the BER of 4-PPM, the BER at 64-PPM with QC-LDPC could meet the threshold requirement of FEC when the Maalox solution concentration is 230.5 mg m^{-3}. In addition, the BERs are lower before the solution concentration of 230.5 mg m^{-3}. This is because under low scattering conditions, more photons carrying the signal enter the detector. In other words, it is more suitable for relatively clear waters for 490 nm laser.

After the solution concentration is increased to 461.1 mg m^{-3}, the scattering solution is continued to increase in order to obtain a lower SNR, as shown in Fig. 12(c). With the further decrease of SNR, BERs also gradually increase. It can still be seen from the trend that the performance of the BERs at 64-PPM and 256-PPM with QC-LDPC is obviously better than other conditions. At this time, under the condition of FEC threshold, the gain of these two types modulation under QC-LDPC is 0.4 dB and 0.35 dB, respectively.

In order to more clearly express the gain brought by QC-LDPC, we measured the power attenuation curve of mode-locked laser under different Maalox solution concentrations, as shown in Fig. 12(d), where the slope of the fitting curve is represented by the black dotted line. Combined with Fig. 12(a) and (d), the power lower limit increases brought by different bit rates (i.e., 1/2, 2/3, 3/4, 5/6 bit rates) compared with no coding are 3.5, 2.8, 2.2, 1.4 dBm, respectively. For modulation, according to Fig. 12 (b) and 12(d), the power detection lower bound gain of 256-PPM compared to 64-PPM and 4-PPM is 5.3 dBm and 8.4 dBm, respectively.

To test the advantages of mode-locked laser in underwater communication, at the transmission distance of 18 m, we measured the BERs performance of CW and mode-locked lasers under QC-LDPC (2304,1152) and 64-PPM, while the underwater attenuation coefficients of CW and mode-locked lasers at different Maalox suspension concentrations are obtained, as shown in Fig. 13(a) and (b), respectively. And both the CW blue light and the mode-locked blue light are all generated from a same laser, whose structure has been shown in Fig. 7 (a). Generally, the laser produces CW light. When the position of the SESAM was adjusted properly, the mode-locked light can be obtained. The wavelength and linewidth of the CW light and the mode-locked light were shown together in Fig. 7(b). At the same time, for the comparability of the experimental results, we also ensure that the power of the CW blue light and the mode-locked blue light are the same.

From the Fig. 13 (a), it can be seen that BERs of two type lasers all increase with the increased of Maalox suspension concentration, because higher concentration improves the forward and backward scattering ability at the underwater communication, and the folded optical path further increase the interference between light beams. In addition, the BERs of mode-locked laser is lower than CW laser in the same condition.

Fig. 13(b) shows the attenuation coefficients that calculated according to Beer-Lambert law at different concentrations. Obviously, the attenuation coefficient of the mode-locked laser is lower than that of the CW laser under the same suspension concentration. This means that mode-locked laser can transmit further at the same average power. For example, when the suspension concentration is 0 mg m^{-3}, the attenuation coefficient of CW laser is 0.128 m^{-1}, the output power of the CW laser should be 3.6 W to achieved 100 m transmission distance, corresponding a received power of 0.01 mW. Comparatively, the attenuation coefficient of mode-locked laser is only 0.08 m^{-1}, it can transmit about 160 m with the same laser power. Even if the power of CW laser is increased by 10 dB, the transmission distance can only be increased to 118 m, and it is a huge challenge for engineering realization.

4. Conclusions

In summary, we have studied the improved characteristics of a passively mode-locked VECSEL based UWOC system including the parameter simulations of QC-LDPC and PPM, the UWOC experiments of mode-locked laser, and the attenuation characteristics of the underwater channel. Through the parameters simulation of QC-LDPC, various values suitable for long-distance underwater communication are obtained, namely, 10 iterations, 2304 code length and 1/2 code rate. Then the UWOC system is built based on a SESAM passively mode-locked VECSEL with the pulse width of 2.25 ps and the repetition rate of 1.46 GHz. Using the PPM, the BER performances of the different concentration Maalox solutions in 18 m underwater channel are investigated under the condition of 20 ns modulation symbol. The results show that with 256-PPM, the received optical power and SNR of QC-LDPC (2304, 1152) are increased by 3.5 dBm and 0.4 dB, respectively. We also measured the underwater channel characteristics of CW and mode-locked VECSEL. According to the attenuation coefficient of the mode-locked VECSEL in different Maalox solutions, the maximum communication distance under the present power is calculated to be 92 m, 56 m, 35 m, 27 m and 23 m (the received optical power is 0.01 mW), respectively, which is 33.7%, 28.6%, 17.1%, 14.8% and 13% higher than the transmission distance of the CW VECSEL.

Declaration of competing interest

The authors declare that they have no known competing financial interests or personal relationships that could have appeared to influence the work reported in this paper.

Data availability

Data will be made available on request.

Acknowledgements

This work is supported by the Cooperation Project between Chongqing Local Universities and Institutions of Chinese Academy of Sciences, Chongqing Municipal Education Commission (HZ2021007), the Science and Technology Research Program of Chongqing Municipal Education Commission (KJQN202200557), the Science and Technology Research Program of Chongqing Municipal Education Commission (KJZD-M201900502), the National Natural Science Foundation of China (61975003, 61790584 and 62025506).

References

[1] P. Agheli, H. Beyranvand, M.J. Emadi, UAV-assisted underwater sensor networks using RF and optical wireless links, J. Lightwave Technol. 39 (22) (2021) 7070–7082.
[2] J. Heidemann, M. Stojanovic, M. Zorzi, Underwater sensor networks: applications, Advances, and Challenges, Phil. Trans. R. Soc. A. 370 (2012) 158–175.
[3] Y. Weng, Y. Guo, O. Alkhazragi, T.K. Ng, J.-H. Guo, B.S. Ooi, Impact of turbulent-flow-induced scintillation on deep-ocean wireless optical communication, J. Lightwave Technol. 37 (19) (2019) 5083–5090.
[4] B.D. Deebak, F. Al-Turjman, Aerial and underwater drone communication: potentials and vulnerabilities, in: Drones in Smart-Cities, Elsevier, 2020, pp. 1–26.
[5] Z. Zeng, S. Fu, H. Zhang, Y. Dong, J. Cheng, A survey of underwater optical wireless communications, IEEE Commun. Surv. Tut. 19 (1) (2016) 204–238.
[6] C. Zhang, Y. Zhang, Z. Tong, H. Zou, H. Zhang, Z. Zhang, G. Lin, J. Xu, Theoretical analysis and experimental demonstration of gain switching for a PPM based UWOC system with picosecond pulses, Opt Express 30 (21) (2022) 38663–38673.
[7] J. Hou, P.H. Siegel, L.B. Milstein, Performance analysis and code optimization of low-density parity-check codes on Rayleigh fading channels, IEEE J. Sel. Area. Commun. 19 (5) (2001) 924–934.
[8] J. Anguita, I. Djordjevic, M. Neifeld, B. Vasic, Shannon capacities and error-correction codes for optical atmospheric turbulent channels, J. Opt. Netw. 4 (9) (2005) 586–601.
[9] I.B. Djordjevic, B. Vasic, M.A. Neifeld, LDPC coded OFDM over the atmospheric turbulence channel, Opt Express 15 (10) (2007) 6336–6350.
[10] Y. Chen, M. Kong, T. Ali, J. Wang, R. Sarwar, J. Han, C. Guo, B. Sun, N. Deng, J. Xu, 26 m/5.5 Gbps air-water optical wireless communication based on an OFDM-modulated 520-nm laser diode, Opt Express 25 (13) (2017) 14760–14765.
[11] H.-H. Lu, C.-Y. Li, H.-H. Lin, W.-S. Tsai, C.-A. Chu, B.-R. Chen, C.-J. Wu, An 8 m/9.6 Gbps underwater wireless optical communication system, IEEE Photon. J. 8 (5) (2016) 1–7.
[12] T.-C. Wu, Y.-C. Chi, H.-Y. Wang, C.-T. Tsai, G.-R. Lin, Blue laser diode enables underwater communication at 12.4 Gbps, Sci Rep-UK 7 (1) (2017) 1–10.
[13] T.Y. Elganimi, Performance comparison between OOK, PPM and pam modulation schemes for free space optical (FSO) communication systems: analytical study, Int. J. Comput. 79 (11) (2013) 22–27.
[14] Q. Tang, L. Yang, G.B. Giannakis, T. Qin, Battery power efficiency of PPM and FSK in wireless sensor networks, IEEE Trans. Wireless Commun. 6 (4) (2007) 1308–1319.
[15] F. Qu, L. Yang, A. Swami, Battery power efficiency of PPM and OOK in wireless sensor networks, ICASSP 3 (2007). III-525-III-528.
[16] G.A. Mahdiraji, E. Zahedi, Comparison of selected digital modulation schemes (OOK, PPM and DPIM) for wireless optical communications, in: 2006 4th Student Conference on Research and Development, 2006, pp. 5–10.
[17] S. Hu, L. Mi, T. Zhou, W. Chen, 35.88 attenuation lengths and 3.32 bits/photon underwater optical wireless communication based on photon-counting receiver with 256-PPM, Opt Express 26 (17) (2018) 21685–21699.
[18] J. Shen, J. Wang, X. Chen, C. Zhang, M. Kong, Z. Tong, J. Xu, Towards power-efficient long-reach underwater wireless optical communication using a multi-pixel photon counter, Opt Express 26 (18) (2018) 23565–23571.
[19] Q.-R. Yan, M. Wang, W.-H. Dai, Y.-H. Wang, Synchronization scheme of photon-counting underwater optical wireless communication based on PPM, Opt Commun. 495 (2021), 127024.
[20] J. Huang, C. Li, J. Dai, R. Shu, L. Zhang, J. Wang, Real-time and high-speed underwater photon-counting communication based on SPAD and PPM symbol synchronization, IEEE Photon. J. 13 (5) (2021) 1–9.
[21] C. Zhang, X. Yang, H. Zou, H. Zhang, Y. Zhang, Y. Dai, G. Song, Z. Zhang, B. Wu, J. Xu, 9.14-Mbps 64-PPM UWOC system based on a directly modulated MOPA with pre-pulse shaping and a high-sensitivity PMT with analog demodulation, Opt Express 30 (17) (2022) 30233–30245.
[22] R. Chen, Z. Lv, Y. Li, C. Qiu, Z. Liu, P-3.19: demonstration of underwater wireless optical communication system using a green micro-LED and FPGA-based PPM modulation, in: SID Symposium Digest of Technical Papers, vol. 53, 2022, pp. 732–734, s1.
[23] C.D. Mobley, B. Gentili, H.R. Gordon, Z. Jin, G.W. Kattawar, A. Morel, P. Reinersman, K. Stamnes, R.H. Stavn, Comparison of numerical models for computing underwater light fields, Appl. Opt. 32 (36) (1993) 7484–7504.
[24] L. Mullen, A. Laux, B. Cochenour, Propagation of modulated light in water: implications for imaging and communications systems, Appl. Opt. 48 (14) (2009) 2607–2612.
[25] M. Kuznetsov, F. Hakimi, R. Sprague, A. Mooradian, High-power (> 0.5-W CW) diode-pumped vertical-external-cavity surface-emitting semiconductor lasers with circular TEM00 beams, IEEE Photon. Technol. Lett. 9 (8) (1997) 1063–1065.
[26] A. Tropper, S. Hoogland, Extended cavity surface-emitting semiconductor lasers, Prog. Quant. Electron. 30 (1) (2006) 1–43.
[27] A. Rahimi-Iman, Recent advances in VECSELs, J. Optics-UK 18 (9) (2016), 093003.
[28] M. Guina, A. Rantamäki, A. Härkönen, Optically pumped VECSELs: review of technology and progress, J. Phys. D Appl. Phys. 50 (38) (2017), 383001.
[29] B. Rudin, A. Rutz, M. Hoffmann, D. Maas, A.-R. Bellancourt, E. Gini, T. Südmeyer, U. Keller, Highly efficient optically pumped vertical-emitting semiconductor laser with more than 20 W average output power in a fundamental transverse mode, Opt. Lett. 33 (22) (2008) 2719–2721.
[30] B. Heinen, T. Wang, M. Sparenberg, A. Weber, B. Kunert, J. Hader, S. Koch, J. Moloney, M. Koch, W. Stolz, 106 W continuous-wave output power from vertical-external-cavity surface-emitting laser, Electron. Lett. 48 (9) (2012) 1.
[31] T. Wang, B. Wang, L. Liu, R. Zhu, L. Wang, C. Tong, Y. Song, P. Zhang, 15 Mbps underwater wireless optical communications based on acousto-optic modulator and NRZ-OOK modulation, Opt Laser. Technol. 150 (2022), 107943.
[32] Tian, H. Chen, P. Wang, X. Liu, X. Chen, G. Zhou, S. Zhang, J. Lu, P. Qiu, Z. Qian, Absorption and scattering effects of Maalox, chlorophyll, and sea salt on a micro-LED-based underwater wireless optical communication, Chin. Opt Lett. 17 (10) (2019), 100010.
[33] J.W. Ren, D. Hou, Y.F. Gao, G.K. Guo, K. Liu, Highly stable multiple-access underwater frequency transfer with terminal phase compensation, Opt. Lett. 46 (19) (2021) 4745–4748.
[34] X.T. Han, P. Li, G.Y. Li, C. Chang, S.W. Jia, Z. Xie, X. Xie, Demonstration of 12.5 mslot/s 32-PPM underwater wireless optical communication system with 0.34 photons/bit receiver sensitivity, Photonics 10 (4) (2023) 451.
[35] B. Cochenour, K. Dunn, A. Laux, L. Mullen, Experimental measurements of the magnitude and phase response of high-frequency modulated light underwater, Appl. Opt. 56 (14) (2017) 4019–4024.
[36] D.T. Nguyen, Y. Park, Performance analysis of interleaved LDPC for optical satellite communications, Opt Commun. 442 (2019) 13–18.